Eur. Phys. J. Appl. Phys. **89**, 10302 (2020)

https://doi.org/10.1051/epjap/2020190265

THE EUROPEAN PHYSICAL JOURNAL APPLIED PHYSICS

Regular Article

Photoconductivity kinetics of indium sulfofluoride thin films★

Yuri Vygranenko[1,*], Miguel Fernandes[1,2], Manuela Vieira[1,2], Guilherme Lavareda[1,3], Carlos Nunes de Carvalho[3,4], Pedro Brogueira[4,5], and Ana Amaral[4,5]

[1] CTS-UNINOVA, Quinta da Torre, 2829-516 Caparica, Portugal
[2] Departamento de Engenharia Electrónica e Telecomunicações e de Computadores, ISEL, Lisboa, Portugal
[3] Departamento de Ciência dos Materiais, Faculdade de Ciências e Tecnologia, Universidade Nova de Lisboa, Liston, Portugal
[4] CeFEMA, Instituto Superior Técnico, Universidade de Lisboa, Liston, Portugal
[5] Departamento de Física, Instituto Superior Técnico, Universidade de Lisboa, Liston, Portugal

Received: 2 September 2019 / Received in final form: 2 December 2019 / Accepted: 17 February 2020

Abstract. Indium sulfofluoride is an amorphous wide-gap semiconductor exhibiting high sensitivity to UV radiation. This work reports on the kinetics of photoconductivity in indium sulfofluoride thin films along with their electrical and optical properties. The films were deposited by radio-frequency plasma-enhanced reactive thermal evaporation. The film characterization includes electrical, optical, and photoconductivity measurements. The films are highly transparent in the visible-infrared range due to an indirect bandgap of 2.8 eV. The spectral response measurements have revealed existence of the band tail states. The synthesized compound is highly resistive (~200 MΩ-cm at 300 K) and exhibits extremely slow photocurrent relaxations. Photoconductivity kinetics was studied under various excitation conditions. A dependence of the photocurrent on the incident photon flux was also determined.

1 Introduction

Disordered semiconductors such as hydrogenated amorphous silicon and its alloys [1], chalcogenide glassy semiconductors [2], amorphous oxide semiconductors [3] are used in various fields of electronics due to possibility to make devices of large area and low cost. Besides, a number of unique effects are observed in these materials that allows creation of devices on the new principles. The development of new materials with such unique properties is a need for various applications in modern technology.

Recently, we reported on indium sulfofluoride ($In_{1-x-y}S_xF_y$) thin films deposited by plasma-enhanced reactive thermal evaporation (rf-PERTE) [4]. The synthesized material is an amorphous wide-gap semiconductor exhibiting high sensitivity to UV radiation. Also this material has been developed targeting its use as a buffer layer in chalcogenide-based solar cells, other light-sensing applications are also prospective. However, more detailed study on photoconductive properties of $In_{1-x-y}S_xF_y$ should be done for practical applications.

In this paper, we report on kinetics of photoconductivity in $In_{1-x-y}S_xF_y$ films along with their electrical and optical properties. The detailed description of film preparation and characterization techniques is the starting point of the presented work. This follows with analysis of optical absorption in the interband and sub-bandgap regions. Then, we demonstrate and discuss the effect of charge trapping on the temperature dependencies of resistivity. After that, the study is focused on the transient photocurrent experiments performed under various excitation conditions. We have also attempted to interpret our experimental results in the frame of known photoconductivity models.

2 Experimental details

2.1 $In_{1-x-y}S_xF_y$ films preparation

The films for this study were prepared using an automated rf-PERTE system described in details elsewhere [5]. The deposition was performed evaporating pure indium in a SF_6 plasma on fused silica and Corning glass substrates. The deposition conditions were 4×10^{-2} Pa pressure, 12 sccm gas flow, 40 W rf-power, 130 °C substrate temperature, and a deposition rate of about 0.2 nm/s. The film thickness was determined by a Veeco Dektak III. It was in the range of 280–330 nm due to deposition non-uniformity within an area of 10 × 10 cm. Samples for electrical characterization were prepared by evaporating Al through a shadow mask to form coplanar contacts with 0.73 mm channel length.

2.2 Characterization techniques

The transmittance in the visible and near violet/infra-red regions (200–2200 nm) was measured using a Shimadzu UV-3100 spectrophotometer, without a bare substrate

★ Contribution to the Topical Issue "Disordered Semiconductors: Physics and Applications", edited by Jean-Paul Kleider, Erik Johnson, Rudolf Brüggemann.

* e-mail: yvygranenko@deetc.isel.ipl.pt

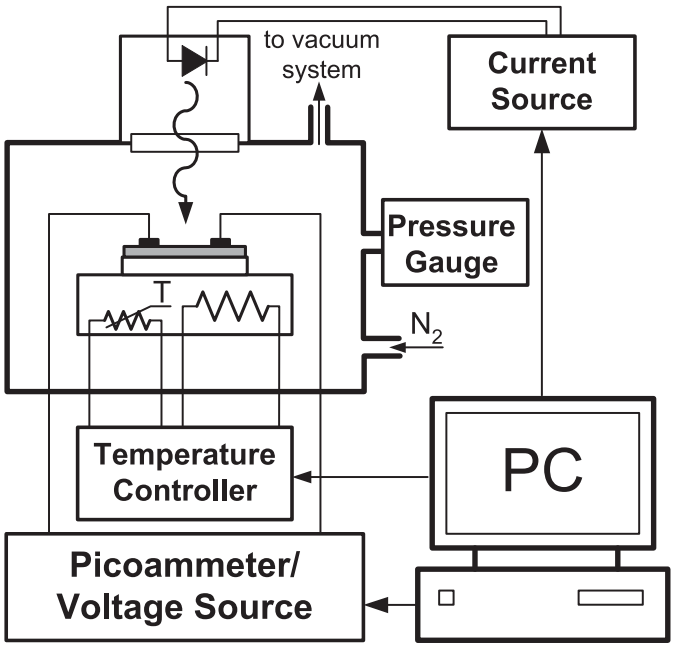

Fig. 1. Schematic diagram of a photoconductivity measurement setup.

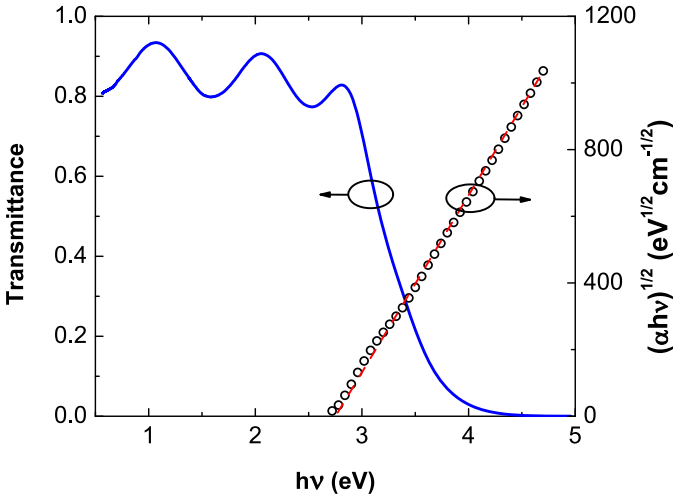

Fig. 2. Transmission spectrum and Tauc's plot.

across the reference beam. The spectral response measurements were performed using a PC controlled setup based on a Triax-120 grating monochromator, a Stanford Research System SR540 light chopper, and a SR530 DSP lock-in amplifier. The system was calibrated in the spectral range of 300–1100 nm using a Thorlabs FDS1010-CAL detector.

The computer-controlled setup used for photoconductivity measurements is shown schematically in Figure 1. It comprises a vacuum chamber with a heater, an Omron E5CC-CX3A5M digital temperature controller with a Pt100 thermoresistor, a Keithley 6487 picoammeter/voltage source, a LED controlled by a Keithley 2400 source-meter, and Thyracont VSC42-MA4 pressure gauge. All electronic units are linked to a computer through RS-232 and RS-485 ports that enables the temperature and incident light flux control using dedicated software. The temperature dependencies were measured in the nitrogen atmosphere at 80 mbar pressure to avoid oxidation and photochemical reactions. Transient photoconductivity measurements were performed using a GaN LED with 398 nm peak emission to reach quasi-uniform excitation of the film bulk within the region of fundamental absorption.

3 Results and discussion

3.1 Optical absorption

Figure 2 shows the transmission spectrum and Tauc's plot assuming indirect nature of the band gap for $In_{1-x-y}S_xF_y$. The absorption coefficient α was determined in the region of strong absorption using the method proposed in reference [6]. The optical thickness of the film obtained in the transparent region is 315 nm that is consistent with the profilometer data reported above. The band gap of 2.76 eV is determined by fitting the linear part of the $(\alpha h\nu)^{1/2}$ curve and calculating the intercept with the energy-axes at $\alpha = 0$. The deduced value is greater than 2.24 eV indirect bandgap energy reported for β-In_2S_3 single crystals [7]. This can be explained by high fluorine content or/and strong structural disorder in $In_{1-x-y}S_xF_y$. Another example of impurity-induced band gap widening is In_2S_3:Na exhibiting a band gap increase of approximately 450 meV at the highest investigated sodium content [8]. Note that the as-deposited In_2S_3:Na films are amorphous and become nanocrystalline after thermal annealing at 673 K [9].

The absorption coefficient in the sub-bandgap region was obtained from a photoconductivity spectrum measured at a chopping frequency of 6 Hz. Applying the same experimental conditions, the photocurrent I_{ph} as a function of the incident photon flux F was also measured in the range covering the spectral-response signal. Note that the sample was unintentionally exposed to ambient light before these measurements causing the long-term (much longer than the experiment time, see next section) photocurrent component of about 10 nA that was significantly higher than the measured *ac* signal. Figure 3 shows $I_{ph} = f(F)$ curves plotted on a *log–log* scale for 2.0 and 2.5 eV photon energies. The intensity dependence may be expressed as

$$I_{ph} \sim F^{\gamma}, \tag{1}$$

where γ is the empirical exponent. The deduced values of γ are 0.96 and 0.94 for 2.0 and 2.5 eV curves, respectively. With known γ, the spectral-response data $I_{ph}(h\nu, F)$ can be applied to calculate the low-energy absorption coefficient by [10]

$$\frac{\alpha(h\nu)}{\alpha_0} = \frac{F_0}{F}\left(\frac{I_{ph}(h\nu, F)}{I_{ph0}}\right)^{1/\gamma} \tag{2}$$

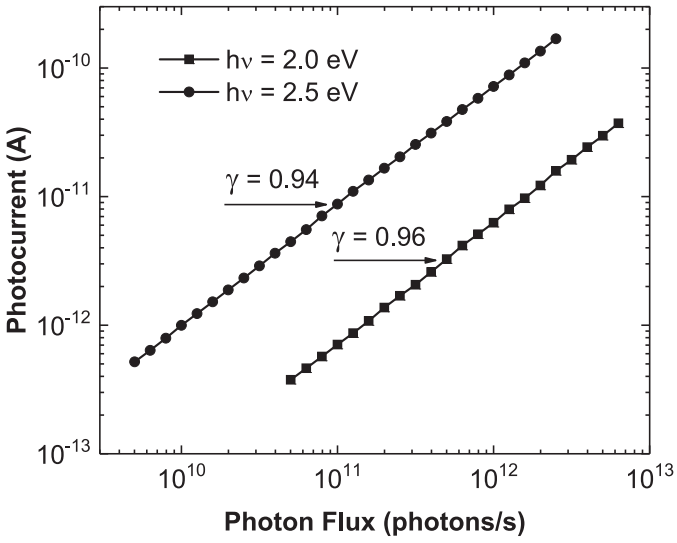

Fig. 3. Variation of *ac* photocurrent component with incident flux of 2 and 2.5 eV photons. The chopping frequency is 6 Hz.

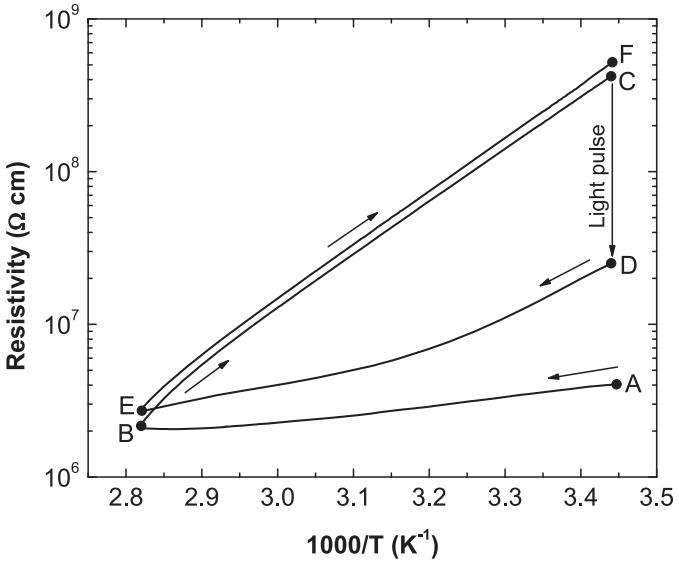

Fig. 5. Temperature dependence of resistivity of the $In_{1-x-y}S_xF_y$ film.

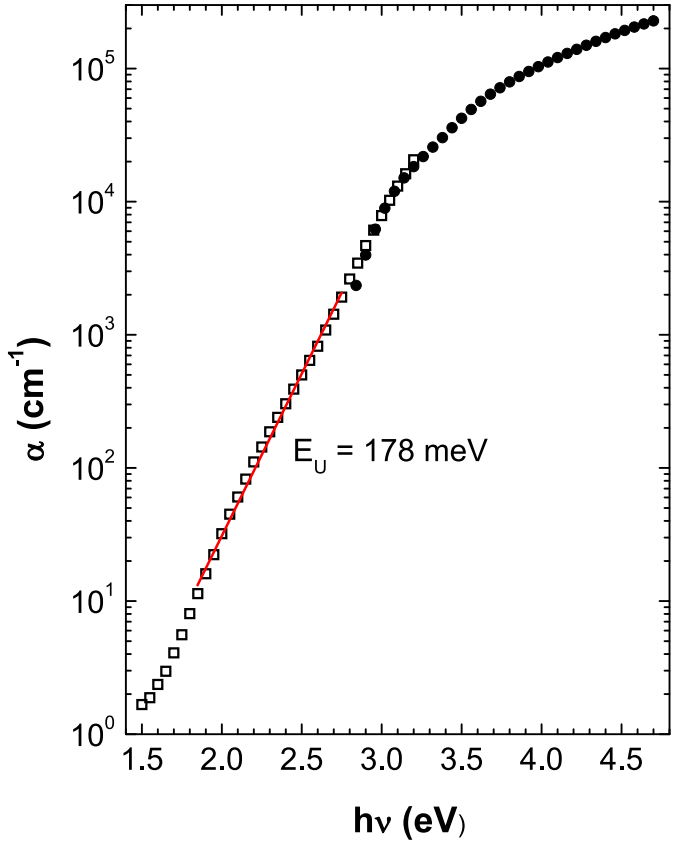

Fig. 4. Absorption coefficient α versus photon energy $h\nu$ derived from photoconductivity (squares) and transmission (circles) measurements.

where the subscript 0 refers to some reference energy $h\nu_0$, and α_0 is the absorption coefficient at $h\nu_0$. Figure 4 shows the calculated $\alpha(h\nu)$ values (squares) by equation (2) along with data derived from the transmittance spectra (circles). The upper limit for the photoconductivity data is determined by $\alpha d_f < 1$ condition, where d_f is the film thickness, while the deduced transmission data are accurate at $h\nu > E_g$. The two sets of data overlap in 2.8–3.3 eV photon energy range with a good match between the curves. At $h\nu \leq E_g$, the absorption coefficient decreases exponentially over 3 orders of magnitude that can be attributed to optical transitions involving the band tail states. The deduced Urbach energy is 178 meV.

3.2 Temperature dependencies of resistivity

Figure 5 shows the dependencies of $\log(\rho)$ with inverse of temperature for the $In_{1-x-y}S_xF_y$ thin film. The measurements were performed at heating/cooling rate of about 20 mK/s in the range of 290–355 K. Curve AB corresponds to a low-resistance state due to the trapped charge since the sample was exposed to light before mounting into the light-shielded vacuum chamber. When the sample is cooled (curve BC), the film resistivity follows the $\rho \sim \exp(E_a/kT)$ relation, yielding $E_a = 693$ meV and $\rho_{300K} = 210$ MΩ cm. Then, the film is switched to the low-resistance state by 1 s light pulse (transition C → D) and heating-cooling cycle D − E − F is repeated again. Also the trapped charges are different in these cycles (initial points A and D), the slopes of curves AB and EF are almost the same. Thus, quenching of persistent photoconductivity can be done by heating the film above some critical temperature and cooling.

3.3 Photoconductivity kinetics

Figure 6 shows the photocurrent transients after 2 s light pulse at a temperature of 20 °C. The fast and slow decay components can be distinguished here. At $t > 60$ s, the slow decay obeys the power law relation $I_{ph} \sim t^{-\beta}$, with $\beta = 0.415$. The estimated time for reaching the initial dark

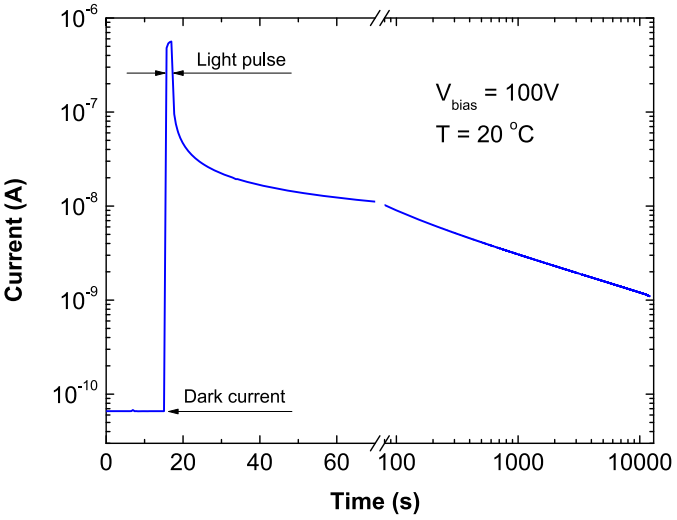

Fig. 6. Photoresponse on 2 s light pulse.

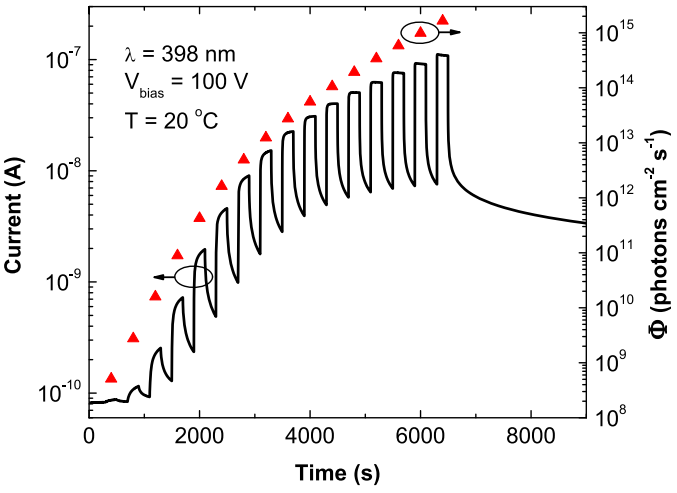

Fig. 7. Photoresponse to 200 s light pulses. The photon flux density is shown for each pulse (triangles).

current value is about 129 days. The transient photocurrent experiments were also performed at various temperatures up to 77 °C yielding about the same $\beta = 0.41 \pm 0.02$.

The power-law decay is typical for amorphous semiconductors. In particular, in the presence of a simple exponential trap distribution of characteristic energy $E_{ct} = kT_C$, two power-law regimes are predicted for monomolecular recombination [11]:

$$I_{ph} \sim t^{-(1-a)}, \tag{3}$$

and

$$I_{ph} \sim t^{-(1+a)}, \tag{4}$$

where $a = T/T_C$ is the dispersion parameter. At short times, in the pre-recombination regime (Eq. (3)), the electrons thermalizes without loss by trapping in the distribution of localized states in the gap. The post-recombination regime (Eq. (4)) occurs when the probability for recombination of free electrons exceeds that for further, deeper trapping in the distribution. Thus, a power law exponent ($\beta = 1+a$) of greater than unity is expected for the long time decay. However, the measured value is less than unity that appears to be problematic. To resolve the contradiction, it should be accepted that the deep part of the density of states involved in trapping must rise toward the middle of the gap leading to negative E_{ct} [12]. In our case, for $\beta = 0.415$ at $T = 293$ K, the characteristic energy is to be about −44 meV (or $T_C = -500$ K). Another inconsistency is that the model predicts a linear dependency of the exponent on temperature, but in fact β is a constant in the measured temperature range.

Measurements of transient photocurrents were also performed at the excitation levels varied from 3×10^9 to 1.7×10^{15} photons $\cdot$ cm^{-2} s^{-1}. Figure 7 shows the photoresponse to a series of 200 s light pulses. The respective values of the incident photon flux density (Φ) for each pulse are also shown in the plot (triangles). At low

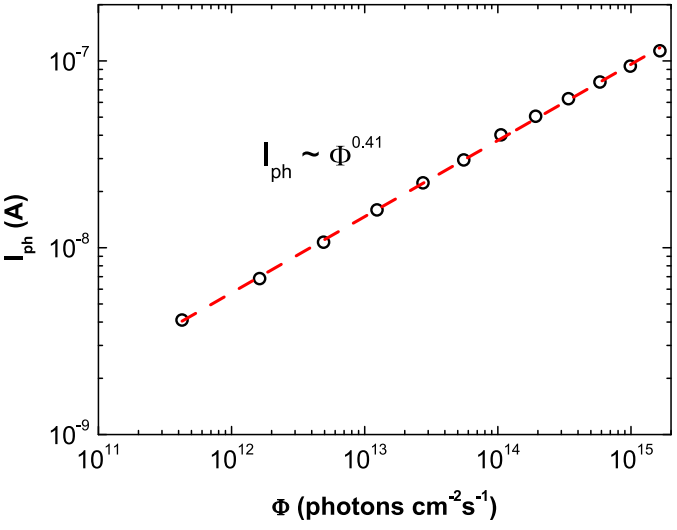

Fig. 8. Steady-state photocurrent as a function of photon flux density Φ.

excitation levels the signal slowly rises and decays due to trapping/release of induced charges. Only at $\Phi > 10^{13}$ photons cm^{-2} s^{-1} the signal saturates within the illumination period, followed by the photocurrent decay with fast and slow components. The deduced peak photocurrent values are plotted against the incident photon flux densities on a log–log scale (Fig. 8). The data follow the relation $I_{ph} \sim \Phi^{\gamma}$. The exponent $\gamma = 0.41$ is obtained as a slope of the indicated linear fit. In amorphous semiconductors, γ is typically ranging from 0.5 to 1 depending on the illumination level, temperature, and related recombination mechanism. The obtained value is even less than $\gamma = 0.5$, which is associated with a bimolecular recombination process. Values of gamma as low as 0.42 have been reported by Main et al. for n-type a-Si:H at about 200 K [13]. They propose that while recombination takes place via defect states, the rate-limiting step is imposed by

charge neutrality, involving as a key element hole emission from an exponential valence band tail state distribution of characteristic energy kT_v. At high generation rates, their model predicts $\gamma = kT_c \,/\, kT_v$, where kT_c is the conduction band characteristic energy. In our case, the observed $\gamma = 0.41$ and $kT_v = 178$ meV indicates $kT_c = 73$ meV, which seems plausible. However, other predictions such as the presence of a strongly sub-linear photocurrent-flux relationship down to very low photocurrents (below the dark current) are contrary to our results. At present therefore, we cannot confirm the applicability of this model.

4 Conclusion

$In_{1-x-y}S_xF_y$ thin-films have been deposited by the rf-PERTE technique. The synthesized material is a highly resistive amorphous semiconductor with an indirect optical band gap of 2.8 eV. The photoconductivity spectrum in the sub-bandgap energy range indicates presence of the band tail states with a characteristic energy of about 180 meV. The material exhibits persistent photoconductivity that significantly exceeds dark conductivity in a time scale of days. Quenching of persistent photoconductivity was done by heating the film up to 80 °C and cooling. The kinetics of the long-term photocurrent decay can be described by the relation $I_{ph} \sim t^{-\beta}$, with $\beta = 0.41$. Relaxation of pulsed photocurrents under various excitation levels was also studied. The obtained dependence of photocurrent on the photon flux follows to $I_{ph} \sim \Phi^{\gamma}$, with $\gamma = 0.41$ for high excitation. The experimental results cannot be explained in the frame of a multiple-trapping model, and further research is needed to understand the nature of persistent photoconductivity.

This research is supported by EU funds through the FEDER European Regional Development Fund and by Portuguese national funds by FCT – Fundação para a Ciência e a Tecnologia with project PhotoAKI: PTDC/NAN-OPT/31311/2017, IPL/2019/BioPlas-ISEL, and pluriannual contract with CeFEMA (UID/CTM/04540/2019).

Author contribution statement

G. Lavareda and C. Nunes de Carvalho deposited the thin-films. Y. Vygranenko and M. Fernandes carried out the electrical and optical measurements. M. Vieira, P. Brogueira, and A. Amaral were involved in supervising the project and contributed to the interpretation of the results. Y. Vygranenko wrote the manuscript with input from all authors.

References

1. R.A. Street, *Technology and Applications of Amorphous Silicon* (Springer-Verlag, Berlin, 2000)
2. A. Popov, *Disordered semiconductors: physics and applications* (Pan Stanford Publishing Pte. Ltd., Singapore, 2011)
3. J.E. Medvedeva, D.B. Buchholz, R.P.H. Chang, Adv. Electron. Mater. **3**, 1700082 (2017)
4. Y. Vygranenko, M. Vieira, G. Lavareda, C. Nunes de Carvalho, P. Brogueira, A. Amaral, N.P. Barradas, E. Alves, Thin Solid Films **671**, 49 (2019)
5. M. Fernandesa, Y. Vygranenko, M. Vieira, G. Lavareda, C. Nunes de Carvalho, A. Amaral, Energy Proc. **102**, 96 (2016)
6. R. Swanepoel, J. Phys. E: Sci. Instrum. **16**, 1214 (1983).
7. S.H. Choe, T.H. Bang, N.O. Kim, H.G. Kim, C.I. Lee, M.S. Jin, S.K. Oh, W.T. Kim, Semicond. Sci. Technol. **16**, 98 (2001)
8. J. Schoneberg, M. Richter, J. Ohlanda, P. Eraerds, T. Daliborb, J. Parisi, Thin Solid Films **633**, 243 (2017)
9. N. Barreau, J.C. Bernède, C. Deudon, L. Brohan, S. Marsillac, J. Cryst. Growth **241**, 4 (2002)
10. G. Moddel, D.A. Anderson, W. Paul, Phys. Rev. B **22**, 1918 (1980)
11. J. Orenstein, M.A. Kastner, V. Vaninov, Philos. Mag. B **46**, 23 (1982)
12. C. Main, S. Reynolds, R. Brüggemann, Phys. Status Solidi C **1**, 1194 (2004)
13. C. Main, F. Dick, S. Reynolds, W. Gao, R.A.G. Gibson, J. Non-Cryst. Solids **198**, 263 (1996)

Cite this article as: Yuri Vygranenko, Miguel Fernandes, Manuela Vieira, Guilherme Lavareda, C.Nunes de Carvalho, Pedro Brogueira, Ana Amaral, Photoconductivity kinetics of indium sulfofluoride thin films, Eur. Phys. J. Appl. Phys. **89**, 10302 (2020)